Biochimica et Biophysica Acta 1828 (2013) 1938–1952

Contents lists available at SciVerse ScienceDirect

Biochimica et Biophysica Acta

journal homepage: www.elsevier.com/locate/bbamem

N-Terminal AH2 segment of protein NS4B from hepatitis C virus. Binding to and interaction with model biomembranes

M. Francisca Palomares-Jerez [a], Henrique Nemesio [a], Henri G. Franquelim [b], Miguel A.R.B. Castanho [b], José Villalaín [a,*]

[a] Instituto de Biología Molecular y Celular, Universidad Miguel Hernández, E-03202 Elche-Alicante, Spain
[b] Instituto de Medicina Molecular, Faculdade de Medicina, Universidade de Lisboa, Lisboa, Portugal

ARTICLE INFO

Article history:
Received 30 January 2013
Received in revised form 19 April 2013
Accepted 22 April 2013
Available online 29 April 2013

Keywords:
HCV
NS4B
Phospholipid
Membrane

ABSTRACT

HCV NS4B, a highly hydrophobic protein involved in the alteration of the intracellular host membranes forming the replication complex, plays a critical role in the HCV life cycle. NS4B is a multifunctional membrane protein that possesses different regions where diverse and significant functions are located. One of these important regions is the AH2 segment, which besides being highly conserved has been shown to play a significant role in NS4B functioning. We have carried out an in-depth biophysical study aimed at the elucidation of the capacity of this region to interact, modulate and disrupt membranes, as well as to study the structural and dynamic features relevant for that disruption. We show that a peptide derived from this region, $NS4B_{AH2}$, is capable of specifically binding phosphatidyl inositol phosphates with high affinity, and its interfacial properties suggest that this segment could behave similarly to a pre-transmembrane domain partitioning into and interacting with the membrane depending on the membrane composition and/or other proteins. Moreover, $NS4B_{AH2}$ is capable of rupturing membranes even at very low peptide-to-lipid ratios and its membrane-activity is modulated by lipid composition. $NS4B_{AH2}$ is located in a shallow position in the membrane but it is able to affect the lipid environment from the membrane surface down to the hydrophobic core. The NS4B region where peptide $NS4B_{AH2}$ resides might have an essential role in the membrane replication and/or assembly of the viral particle through the modulation of the membrane structure and hence the replication complex.

1. Introduction

Hepatitis C virus (HCV) is an enveloped positive single-stranded RNA virus, included in the genus *Hepacivirus* of the Flaviviridae family. HCV is the major cause of liver diseases, including steatosis, fibrosis, cirrhosis and hepatocellular carcinoma, and is the leading indication for liver transplantation [1]. With approximately 170 to 200 million people infected worldwide and no protective vaccine available at present HCV has emerged as a serious global health problem, since an estimated 2%–3% of the world population is afflicted by this illness [2,3]. HCV entry into the host cell is achieved by the fusion of viral and cellular membranes, the replication of its genome occurs in a membrane-associated replication complex, and morphogenesis has been suggested to take place in endoplasmic reticulum (ER) modified membranes [4]. HCV has a single-stranded genome, which encodes a polyprotein cleaved by a combination of cellular and viral proteases to produce the mature structural and non-structural (NS) proteins [5,6]. There are unique ties between the HCV life cycle, lipid metabolism, lipid rafts and specific lipid environments; more specifically, the non-structural protein NS4B is engaged in one way or another with all of them [6,7].

Abbreviations: 14BMP, bis(monomyristoylglycero)phosphate; 18BMP, bis(monooleoylglycero)phosphate; 16-NS, 16-doxyl-stearic acid; 5-NS, 5-doxyl-stearic acid; BPI, bovine liver L-α-phosphatidylinositol; BPS, bovine brain L-α-phosphatidylserine; CF, 5-carboxyfluorescein; Chol, cholesterol; CL, bovine heart cardiolipin; DEPE, 1,2-dielaidoyl-sn-glycero-3-phosphatidylethanolamine; DMPA, 1,2-dimyristoyl-*sn*-glycero-3-phosphatidic acid; DMPC, 1,2-dimyristoyl-*sn*-glycero-3-phosphatidylcholine; DMPG, 1,2-dimyristoyl-*sn*-glycero-3-[phospho-rac-glycerol]; DMPS, 1,2-dimyristoyl-*sn*-glycero-3-phosphatidylserine; DOPC, 1,2-dioleoyl-*sn*-glycero-3-phosphocholine; DPH, 1,6-diphenyl-1,3,5-hexatriene; DPPC, 1,2-dipalmitoyl-*sn*-glycero-3-phosphocholine; DSC, differential scanning calorimetry; DSPC, 1,2-distearoyl-*sn*-glycero-3-phosphocholine; EPA, egg L-α-phosphatidic acid; EPC, egg L-α-phosphatidylcholine; EPG, egg L-α-phosphatidylglycerol; ER, endoplasmic reticulum; ESM, egg sphingomyelin; FD20, fluorescein isothiocyanate–dextran average mol wt 20,000; FD70, fluorescein isothiocyanate–dextran average M_w 59,000–77,000; HCV, hepatitis C virus; LEM, late endosome membrane; LUV, large unilamellar vesicles; MAS, magic angle spinning; MLV, multilamellar vesicles; NMR, nuclear magnetic resonance; NS, non-structural protein; PI4P, brain L-α-phosphatidylinositol-4-phosphate; POPC, 1-palmitoyl-2-oleoyl-*sn*-glycero-3-phosphocholine; PSM, N-palmitoyl-D-erythro-sphingosylphosphorylcholine; TFE, 2,2,2-trifluoroethanol; T_m, temperature of the gel-to-liquid crystalline phase transition; TM, transmembrane domain; TMA-DPH, 1-(4-trimethylammoniumphenyl)-6-phenyl-1,3,5-hexatriene; TPE, egg transphosphatidylated L-α-phosphatidylethanolamine

* Corresponding author at: Instituto de Biología Molecular y Celular, Universidad "Miguel Hernández", E-03202 Elche-Alicante, Spain. Tel.: +34 966 658 762; fax: +34 966 658 758.
E-mail address: jvillalain@umh.es (J. Villalaín).

0005-2736/$ – see front matter © 2013 Elsevier B.V. All rights reserved.
http://dx.doi.org/10.1016/j.bbamem.2013.04.020

NS4B is essential in the HCV replicative process, apart from being the least characterized HCV protein and is a highly hydrophobic membrane protein associated with membranes of an ER-derived modified compartment [8]. The expression of NS4B induces the formation of significant intracellular membrane changes, the so called membranous web [9], which has been postulated to be the HCV RNA replication complex. NS4B is likely an integral membrane protein with several transmembrane domains [10]. NS4B is a multifunctional protein that contains an ATP/GTPase function [11], displays anti-apoptotic activity [12], is palmitoylated in the C-terminal region and its N-terminal domain has a potent polymerization activity [13]. The C-terminal part of NS4B contains two α-helical elements, H1 and H2 which are essential for NS4B self-interaction and the formation of functional HCV replication complexes [14]. Significantly, these segments are able of interacting with membranes [15,16]. The N-terminal part of NS4B contains a structurally resolved amphipathic α-helix, AH2, which has been shown to play an important role in HCV RNA replication, has the potential to traverse the phospholipid bilayer as a transmembrane segment and is supposedly engaged in protein oligomerization [13,17]. Mutations that affect the oligomerization of NS4B disrupted membranous web formation and HCV RNA replication, implying that oligomerization of NS4B is required for the creation of a functional replication complex. NS4B might be the protein responsible for binding to specific lipid domains, such as lipid rafts, and thereby enabling the recruitment or anchoring of other viral proteins in order to form the replication complex [18].

We have recently identified the membrane-active regions of a number of viral proteins by observing the effect of peptide libraries on model membrane integrity, including HCV NS4B [19–23]. These results allowed us to propose the location of different segments in these proteins that should be implicated in protein–lipid and protein–protein interactions. One of those membranotropic segments was located where the AH2 region resides. Considering that the interaction between the highly hydrophobic HCV NS4B protein and membranes is fundamental in the viral RNA replication process, it is natural to think of HCV protein/membrane interaction as an attractive target for antiviral drug development. In this work we report the binding and interaction of a peptide corresponding to the AH2 segment of HCV NS4B protein (peptide $NS4B_{AH2}$) with different membrane model systems. We show that $NS4B_{AH2}$ is a membrane interacting domain, which strongly partitions into and interacts with phospholipid biomembranes, modulates the phospholipid phase behavior and changes its secondary structure upon binding to the membrane, behaving similarly to other described viral pre-transmembrane segments. Furthermore, the $NS4B_{AH2}$ peptide binds specifically to different phosphatidyl inositol phosphates supporting the fact that the NS4B protein might be engaged in a multifunctional way with membrane trafficking. These data will help us to understand the molecular mechanism of viral replication which may lead to new vaccine strategies.

2. Materials and methods

2.1. Materials and reagents

Peptides $NS4B_{AH2}$ with sequence KLEVFWAKHMWNFISGIQYLA (residues 45 to 65, HCV strain 1a_H77 NS4B numbering), $NS4B_{AH2\text{-}His}$ with sequence KLEVFWAKHMWNFISGIQYLAGHHHHHHG and $NS4B_{SCAH2\text{-}His}$ with sequence VNFQFMAISGHEWKLYLAKIWGHHHHHHG, were synthesized with N-terminal acetylation and C-terminal amidation on an automatic multiple synthesizer (Genemed Synthesis, San Antonio, TX, USA). The peptides were purified by reverse-phase high-performance liquid chromatography (Vydac C-8 column, 250 × 4.6 mm, flow rate 1 ml/min, solvent A, 0.1% trifluoroacetic acid, solvent B, 99.9 acetonitrile and 0.1% trifluoroacetic acid) to >95% purity, and its composition and molecular mass were confirmed by amino acid analysis and mass spectroscopy. Since trifluoroacetate has a strong infrared absorbance at approximately 1673 cm^{-1}, which interferes with the characterization of the peptide Amide I′ band [24], residual trifluoroacetic acid, used both in peptide synthesis and in the high-performance liquid chromatography mobile phase, was removed by three lyophilization/solubilization cycles in 10 mM HCl [25]. Peptides were solubilized in water/TFE at 50% (v/v). Bovine brain phosphatidylserine (BPS), bovine liver L-α-phosphatidylinositol (BPI), brain L-α-phosphatidylinositol-4-phosphate (PI4P), cholesterol (Chol), egg L-α-phosphatidylglycerol (EPG), egg L-α-phosphatidic acid (EPA), egg L-α-phosphatidylcholine (EPC), egg sphingomyelin (ESM), egg transphosphatidylated L-α-hosphatidylethanolamine (TPE), tetramyristoyl cardiolipin (CL), 1,2-dimyristoylphosphatidylserine (DMPS), 1,2-dimyristoylphosphatidylcholine (DMPC), 1,2-dimyristoylphosphatidylglycerol (DMPG), 1,2-dimyristoylphosphatidic acid (DMPA), 1,2-dipalmitoyl-*sn*-glycero-3-phosphocholine (DPPC), 1,2-distearoyl-*sn*-glycero-3-phosphocholine (DSPC), 1,2-dioleoyl-*sn*-glycero-3-phosphocholine (DOPC), 1-palmitoyl-2-oleoyl-*sn*-glycero-3-phosphocholine (POPC), 1,2-dielaidoyl-*sn*-glycero-3-phosphatidylethanolamine (DEPE), N-palmitoyl-D-erythro-sphingosylphosphorylcholine (PSM), bis(monomyristoylglycero) phosphate (14BMP), bis(monooleoylglycero)phosphate (18BMP) and liver lipid extract were obtained from Avanti Polar Lipids (Alabaster, AL, USA). The synthetic ER membrane contained EPC/CL/BPI/TPE/BPS/EPA/SM/Chol at a molar ratio of 59:0.37:7.4:18:3.1:1.2:3.4:7.8 [45], the synthetic late endosome membrane (LEM) contained EPC/TPE/BPI/18BMP at a molar ratio of 5:1:1:2 [46], whereas the synthetic $ER^{58:6}$ contained EPC/CL/BPI/TPE/BPS/EPA/ESM/Chol at a molar ratio of 58:6:6:6:6:6:6:6. 5-Carboxyfluorescein (CF, >95% by HPLC), 5-doxyl-stearic acid (5-NS), 16-doxyl-stearic acid (16-NS), deuterium oxide (99.9%), Triton X-100, EDTA and HEPES were purchased from Sigma-Aldrich (Madrid, ES). 1,6-Diphenyl-1,3,5-hexatriene (DPH), and 1-(4-trimethylammoniumphenyl)-6-phenyl-1,3,5-hexatriene (TMA-DPH) were obtained from Molecular Probes (Eugene, OR). All other chemicals were commercial samples of the highest purity available (Sigma-Aldrich, Madrid, ES). Water was deionized, twice-distilled and passed through a Milli-Q equipment (Millipore Ibérica, Madrid, ES) to a resistivity higher than 18 MΩ cm.

2.2. Vesicle preparation

Aliquots containing the appropriate amount of lipid in chloroform/methanol (2:1 vol/vol) were placed in a test tube, the solvents were removed by evaporation under a stream of O_2-free N_2, and finally, traces of solvents were eliminated under vacuum in the dark for >3 h. The lipid films were resuspended in an appropriate buffer and incubated either at 25 °C or 10 °C above the phase transition temperature (T_m) with intermittent vortexing for 30 min to hydrate the samples and obtain multilamellar vesicles (MLV). The samples were frozen and thawed five times to ensure complete homogenization and maximization of peptide/lipid contacts with occasional vortexing. Large unilamellar vesicles (LUV) with a mean diameter of either 0.1 μm or 0.2 μm (CF and FD leakage measurements, respectively) were prepared from MLV by the extrusion method [26] using polycarbonate filters (Nuclepore Corp., Cambridge, CA, USA) as described previously [15]. Small unilamellar vesicles (SUV) were prepared from MLVs as described previously [16]. The phospholipid and peptide concentrations were measured by methods described previously [27,28].

2.3. Acrylamide quenching of Trp emission, quenching with lipophilic depth probes and steady-state fluorescence anisotropy

Aliquots from a 4 M solution of the water-soluble quencher were added to the solution-containing peptide in the presence and absence of liposomes at a peptide/lipid molar ratio of 1:100. The results obtained were corrected for dilution and the scatter contribution was derived from acrylamide titration of a vesicle blank. The data

were analyzed according to the Stern–Volmer equation [29]. Quenching with TMA-DPH and DPH depth probes was made as previously described [30]. Quenching studies with lipophilic probes were performed by successive addition of small amounts of 5-NS or 16-NS in ethanol to peptide samples incubated with LUV. The final concentration of ethanol was kept below 2.5% (v/v) to avoid any significant bilayer alterations. After each addition an incubation period of 15 min was kept before the measurement. The Stern–Volmer quenching constant, K_{SV}, is a measure of the accessibility of Trp to the quencher molecule [30].

2.4. Membrane leakage and peptide binding to vesicles

CF and FD membrane leakage was made as previously described [31]. Leakage was quantified on a percentage basis as previously described [30,32]. Peptide binding to lipid membranes was studied using steady-state fluorescence spectra recorded in a SLM Aminco 8000C spectrofluorometer with excitation and emission wavelengths at 290 and 342 nm, respectively, and 4 nm spectral bandwidths. The data were analyzed and partition coefficients, K_P (i.e. the amount of peptide bound to the bilayer as a fraction of the total peptide present in the system), were obtained as described previously [16].

2.5. Differential scanning calorimetry

MLVs were formed as stated above in 20 mM HEPES, 100 mM NaCl, 0.1 mM EDTA, pH 7.4. The peptide was added to obtain a peptide/lipid molar ratio of 1:15. The final volume was 0.8 ml (0.6 mM lipid concentration), and incubated 10 °C above the T_m of each phospholipid for 1 h with occasional vortexing. Differential scanning calorimetry (DSC) experiments were performed in a VP-DSC differential scanning calorimeter (MicroCal LLC, MA) as described in [15].

2.6. Magic angle spinning (MAS) ^{31}P NMR

Samples were prepared as described above and concentrated by centrifugation (14,000 rpm for 15 min). MAS ^{31}P NMR spectra were acquired on a Bruker 500 MHz Avance spectrometer (Bruker BioSpin, Rheinstetten, Germany) using a Bruker 4-mm broad band MAS probe under both static and MAS conditions (see [15] for further details). Under static conditions, the samples showed a broad asymmetrical signal with a low-frequency peak and a high-frequency shoulder characteristic of bilayer structures (data not shown).

2.7. Infrared spectroscopy

Approximately 25 μl of a pelleted sample in D_2O [15] was placed between two CaF_2 windows separated by 56-μm thick Teflon spacers in a liquid demountable cell (Harrick, Ossining, NY). The spectra were obtained and analyzed as previously described [16,33].

2.8. Lipid overlay assay

Two different nitrocellulose membrane strips, i.e., PIP Array strip (cat. No. P-6100), and Membrane Lipid strip (cat. No. P-6002) from Echelon Biosciences Inc., UT, USA, were used. The bound His-derived peptides were detected on the strips using the protocol stated by the manufacturer. In brief, the strips were blocked using PBS plus 1% non-fat dry milk for 1 h at room temperature, incubated with the peptides overnight at 4 °C, washed six times for 10 min in washing buffer containing PBS plus 0.1% Tween-20 and detected by chemiluminescence using a Penta-His antibody (Qiagen, Germany), anti-mouse IgG-HRP (Sigma, Spain), and ECL Detection reagent (Amersham, GE Healthcare, Spain). The concentration of the peptides in the solution was 20 μg/ml.

2.9. Atomic force microscopy (AFM)

A 1 mM SUV suspension (10 mM HEPES buffer pH 7.4 in NaCl 150 mM) was deposited in the presence of $CaCl_2$ 4 mM on a freshly cleaved mica substrate, as described elsewhere [34,35]. The lipid sample was incubated for 30 min at room temperature. Afterwards, the sample was rinsed at least 10 times with buffer and set to equilibrate for another 30 min at room temperature. Samples were scanned in contact mode on a NanoWizard II equipment (JPK Instruments, Berlin, Germany) mounted on top of an Axiovert 200 inverted optical microscope (Carl Zeiss, Jena, Germany). Measurements were performed using uncoated silicon nitride cantilevers OMCL-TR800PSA-1 from Olympus (Tokyo, Japan) with a typical stiffness of 0.15 N/m. All images, for the peptide concentrations and lipid compositions evaluated, were obtained with the same or close AFM parameter (set-point, scan rate, gain) values. Controls where buffer was added instead of peptide solution were performed with the same incubation times and measurement conditions. The scan rate was 2 Hz and the force applied on the sample was maintained at the lowest possible value by continuously adjusting the set-point and gain during the imaging. Images were acquired with a typical 512 × 512 resolution. Data were analyzed using JPK image processing software Version 3 (JPK Instruments) and Gwyddion Version 2.19 (Czech Metrology Institute).

3. Results

NS4B, due to its highly hydrophobic character, is the least characterized of the HCV proteins and therefore many questions remain unanswered about its structure and function. NS4B is predicted to comprise an N-terminal part, a central part comprising several transmembrane domains and a C-terminal part [8,10,36]. Further, HCV NS4B possesses three amphipathic α-helical segments, one at the N-terminal part of the protein (segment AH2) [17] and two at the C-terminal part (segments H1 and H2) [37]. We have recently identified several membrane-active regions of NS4B, one of them pertaining to the segment where the AH2 segment resides [33]. This segment presents a high water-to-interface transfer free energy region immediately followed by a region of high water-to-bilayer transfer free energy albeit with some overlapping between them (Fig. 1) [10]. As observed in Fig. 1, this region is quite conserved among the different genotypes of HCV; the conservation of this pattern across so many different strains of HCV indicates that this sequence is likely to be an important region in the NS4B protein. The free energy pattern displayed in Fig. 1 is characteristically distinctive of the pre-transmembrane domains (also called stem or membrane-proximal domains) of several viral fusion proteins, characterized by their strong propensity to partition into and interact with membrane interfaces [13,17,23,38–43]. These domains are usually rich in aromatic amino acids and play essential roles in membrane destabilization. Interestingly, it has been reported that this segment plays an important role in HCV RNA replication, interacts with ER derived membranes, has the ability to interact with the phospholipid bilayer and most likely has the capability to transverse the membrane given the right conditions [13,17]. In this work we report the binding and interaction of a peptide corresponding to the AH2 segment of protein NS4B from HCV strain 1a_H77 (peptide $NS4B_{AH2}$, Fig. 1) in aqueous solution and in the presence of different membrane model systems. We have characterized the structural changes taking place in the peptide and in the membrane and have defined it as a membrane interacting domain with remarkable properties.

The ability of the $NS4B_{AH2}$ peptide to interact with membranes was determined from fluorescence studies of the peptide's intrinsic Trp residues [44] using model membranes containing diverse phospholipid compositions (Fig. 1B). The peptide was bound to the membrane surface with high affinity since partition constant values (K_p) in the range 10^5 were obtained for the different phospholipid compositions studied (Table 1). Interestingly, the larger values were found for

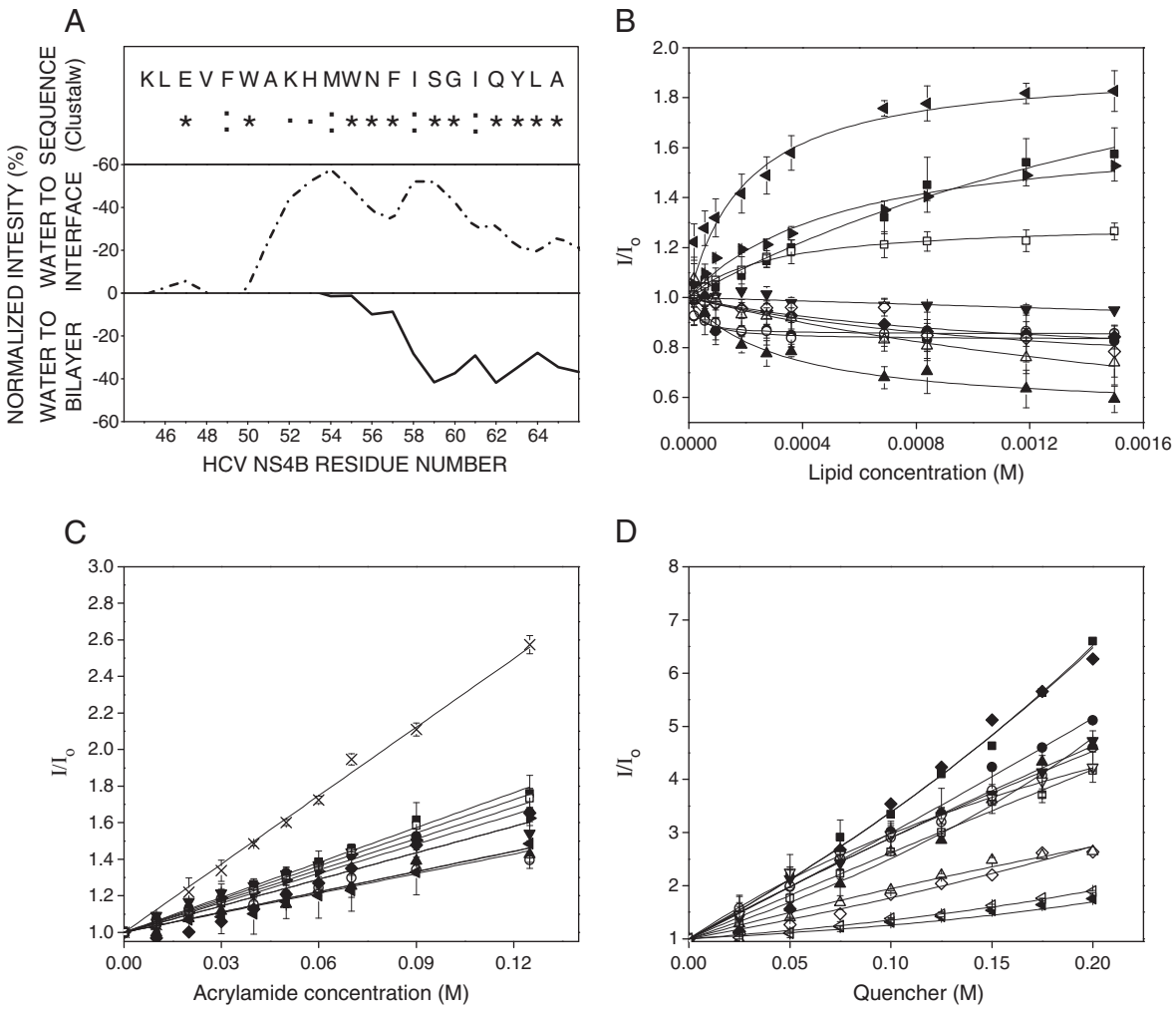

Fig. 1. (A) Average normalized water-to-bilayer (——) and water-to-interface (—·—·—) transfer free energies in kcal/mol for the $NS4B_{AH2}$ peptide (NS4B residues 45 to 65) (see Ref. [10]). Transfer free energies values have been inverted to match the direction of transfer from water-to-bilayer and water-to-interface (the more negative the value, the higher the transfer free energy) [69]. The sequence of the $NS4B_{AH2}$ peptide (HCV strain 1a_H77) and the ClustalW2 alignment corresponding to thirty-one reference HCV strains (sequences 1A_1, 1A_H77, 1B_CON1, 1B_HC-J4, 1C_HC-G9, 1G_1804, 2A_HC-J6, 2B_JPUT971017, 2C_BEBE1, 2I_D54, 2K_VAT96, 3A_NZL1, 3B_TR-KJ, 3K_JK049, 4A_ED43, 4D_24, 4F_CM_DAV9905, 4K_PB65185, 5A_EUH1480, 6A_6A33, 6B_TH580, 6C_TH846, 6D_VN235, 6E_D42, 6F_C-0044, 6G_JK046, 6H_VN004, 6K_VN405, 6O_D85, 6T_D49 and 7A_QC69 were obtained from the HCVdb database, http://www.hcvdb.org/index.asp) are also shown. The similarity of the residues in the alignment is shown below it (identical residues are denoted by *, conserved residues by :, and semi-conserved residues by ·). (B) Change in the fluorescence intensity of the Trp residue of the $NS4B_{AH2}$ peptide in the presence of increasing lipid concentration, (C) Stern–Volmer plots for the quenching of the fluorescence of the Trp residue of the $NS4B_{AH2}$ peptide in the presence of acrylamide and (D) Stern–Volmer plots for the depth-dependent quenching of the fluorescence of the Trp residue of the $NS4B_{AH2}$ peptide in the presence of 5-NS (filled symbols) and (■), EPC/EPA at a molar ratio of 5:2 (▼), EPC/Chol at a molar ratio of 5:1(♦), EPC/BPS at a molar ratio of 5:2 (○), EPC/ESM/Chol at a molar ratio of 5:1:1 (●), EPC/ESM/Chol at a molar ratio of 5:3:1 (□), EPC/BPS/Chol at a molar ratio of 5:2:1 (◊), EPC/EPA/Chol at a molar ratio of 5:2:1 (Δ), liver membranes (▲), synthetic ER membranes (►) and synthetic ER^{586} membranes (◄). Pure peptide in buffer is represented by (×) in panel (C). In (D), the lipid compositions used were EPC (■,□), EPC/ESM/Chol at a molar ratio of 5:1:1 (●,○), EPC/BPS at a molar ratio of 5:2 (♦,◊), EPC/EPA at a molar ratio of 5:2 (▼,▽), liver membranes (▲,Δ) and synthetic ER membranes (◄,◁).Vertical bars indicate standard deviations of the mean of triplicate samples. The lipid to peptide ratio was 100:1 for experiments using acrylamide and both 5- and 16-NS probes.

negatively charged compositions. i.e., liver extract, the $ER^{58:6}$ complex mixture and EPC/BPS at a molar ratio of 5:2, as well as ESM and Chol containing compositions. Stern–Volmer plots for the quenching of Trp by the water-soluble quencher acrylamide [45], recorded in the absence and presence of lipid vesicles, are shown in Fig. 1C and the resultant Stern–Volmer constants are presented in Table 1. The Trp residues were totally accessible to acrylamide since linear Stern–Volmer plots were obtained and in all cases, the quenching of the peptide Trp residues showed an acrylamide dependent concentration behavior. In aqueous solution, the Trp residues were highly exposed to the solvent that led to a more efficient quenching. However, in the presence of the phospholipid membranes, the extent of quenching was significantly reduced, indicating a poor accessibility of the Trp residues to the aqueous phase, consistent with its incorporation into the lipid bilayer. The extent of quenching was much lower in the presence of negatively charged membranes than in membranes containing other phospholipid compositions, in accordance with the results shown above. The transverse location of the $NS4B_{AH2}$ peptide when incorporated in the fluid phase of membranes having different phospholipid compositions was evaluated by monitoring the relative quenching of the fluorescence of the Trp residues by the lipophilic spin probes 5-NS and 16-NS (Fig. 1D). The K_{SV} values for both probes are presented in Table 1. For liposomes composed of EPC, EPC/ESM/Chol at a molar ratio of 5:1:1, the ER complex mixture and EPC/EPA at a molar ratio of 5:2, the differences between the two probes were not very high; however, for membranes composed of the liver extract and the EPC/BPS at a molar ratio of 5:2 differences were significant (Table 1). Combining all these data, we could conclude that the Trp residues are localized in the membrane in between these two probes.

Table 1
Partition coefficients (K_p) and Stern–Volmer quenching constants (K_{SV}) obtained from the fluorescence of the Trp residues of the $NS4B_{AH2}$ peptide in buffer and in the presence of different model membranes.

LUV composition	K_P ($\times 10^{-5}$ M^{-1})	K_{SV} (M^{-1})	K_{SV} (M^{-1})	K_{SV} (M^{-1})
	Trp	Acrylamide	5-NS	16-NS
EPC	0.22 ± 0.07	6.36 ± 0.10	19.74 ± 1.29	16.64 ± 2.03
EPC/Chol 5:1	0.48 ± 0.31	4.83 ± 0.31	–	–
EPC/BPS 5:2	21.6 ± 0.57	3.70 ± 0.19	20.03 ± 2.23	5.88 ± 1.90
EPC/EPA 5:2	0.38 ± 0.05	5.36 ± 0.32	26.57 ± 2.10	28.55 ± 3.22
EPC/ESM/Chol 5:1:1	13.9 ± 3.60	5.69 ± 0.13	18.76 ± 1.68	21.30 ± 2.23
EPC/ESM/Chol 5:3:1	1.98 ± 0.20	6.04 ± 0.10	–	–
ER complex mixture	1.03 ± 0.21	5.42 ± 0.13	1.45 ± 0.59	1.03 ± 0.46
LIVER	1.72 ± 0.30	3.68 ± 0.14	20.87 ± 1.22	11.39 ± 2.91
EPC/BPS/Chol 5:2:1	0.12 ± 0.03	–	–	–
EPC/EPA/Chol 5:2:1	0.20 ± 0.04	–	–	–
$ER^{58:6}$ complex mixture	2.68 ± 0.68	3.57 ± 0.11	–	–
Buffer	–	12.47 ± 0.21	–	–

The effect of the $NS4B_{AH2}$ peptide on the release of encapsulated fluorophores trapped inside model membranes was studied to explore the interaction of the peptide with phospholipid membranes [16]. $NS4B_{AH2}$ was able to induce the release of encapsulated CF in a dose-dependent manner and the effect was significantly different for different lipid compositions (Fig. 2A). The $NS4B_{AH2}$ peptide induced a significant percentage of leakage for liposomes composed of EPC/18BMP at a molar ratio of 5:2, even at a (very high) lipid/peptide ratio of 800:1 the observed leakage was virtually 100% (Fig. 2A). Liposomes composed of EPC or EPC/Chol at a molar ratio of 5:1 elicited significant leakage effects, inducing leakage values of about 85–80% at a lipid/peptide ratio of 800:1. Liposomes composed of negatively charged phospholipids presented lower leakage values. At the lipid/peptide ratio of 800:1, liposomes composed of the LEM and ER complex mixtures, as well as EPC/EPA and EPC/BPS at a molar ratio of 5:2 presented leakage values of 35–25% (Fig. 2A). Chol addition to the LEM composition slightly lowered the observed leakage values (Fig. 2A). Similarly, Chol addition to the EPC/EPA and EPC/BPS compositions lowered leakage significantly, since at lipid/peptide ratio of 200:1 leakage values of 5–10% were observed. Interestingly, liver extract liposomes were the ones that elicited the lowest leakage values, even at high peptide/lipid ratios (Fig. 2A). Fig. 2B shows the extent of

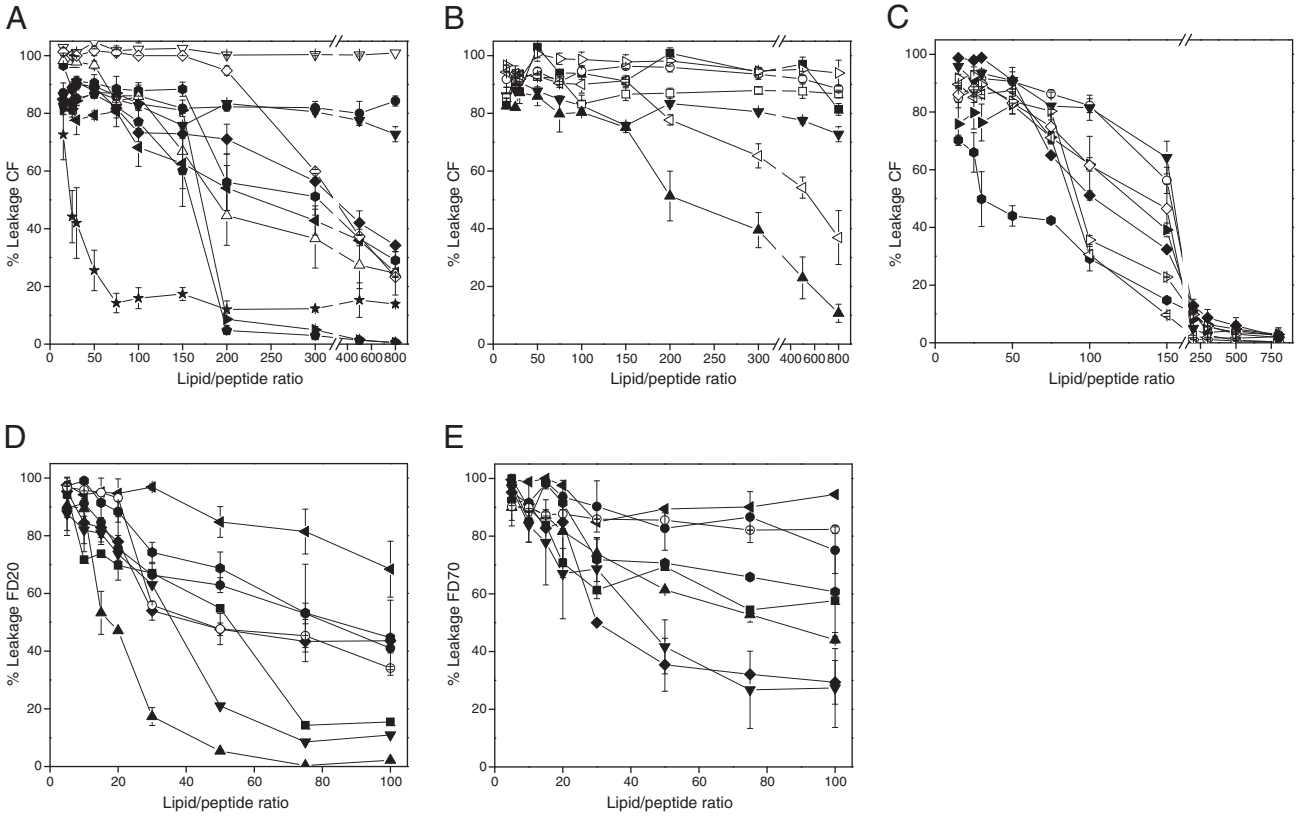

Fig. 2. Effect of the $NS4B_{AH2}$ peptide on the release (membrane rupture) of CF (A, B and C), FD20 (D) and FD70 (E) for general different lipid compositions (A, D and E), lipid compositions containing different molar ratios of EPC, ESM and Chol (B) and the $ER^{58:6}$ complex lipid mixture and its variations (C). The lipid compositions used in (A, B, D and E) were EPC (●), EPC/TPE/BPI/18BMP at a molar ratio of 5:1:1:2 (◊), EPC/TPE/BPI/18BMP/Chol at a molar ratio of 5:1:1:2:2 (Δ), EPC/Chol at a molar ratio of 5:1 (▼), EPC/ESM/Chol at a molar ratio of 5:1:1 (■), EPC/EPA at a molar ratio of 5:2 (♦), liver membranes (★), EPC/ESM at a molar ratio of 5:3 (○), EPC/Chol at a molar ratio of 5:3 (▲), EPC/BPS/Chol at a molar ratio of 5:2:1 (►), EPC/ESM/Chol at a molar ratio of 5:3:1 (□), EPC/18BMP at a molar ratio of 5:2 (▽), EPC/ESM/Chol at a molar ratio 5:1:3 (◁), EPC/BPS at a molar ratio of 5:2 (⬢), EPC/EPA/Chol at a molar ratio of 5:2:1 (⬟), EPC/ESM at a molar ratio of 5:4 (▷), and synthetic ER membranes (◀). The lipid compositions used in (C) were the $ER^{58:6}$ membrane (►), $ER^{58:6}$ minus Chol (▼), $ER^{58:6}$ minus BPI (◊), $ER^{58:6}$ minus TPE (◁), $ER^{58:6}$ minus ESM (▷), $ER^{58:6}$ minus BPS (⬢), $ER^{58:6}$ minus EPA (♦) and $ER^{58:6}$ minus CL (○). Vertical bars indicate standard deviations of the mean of triplicate samples.

leakage for liposomes composed of different molar ratios of EPC, ESM and Chol. The highest leakage values were found for lipid compositions containing the highest ESM proportions: leakage values of 93% and 89% were observed for lipid compositions of EPC/ESM at molar ratios of 5:4 and 5:3 at a lipid/peptide ratio of 800:1. The inclusion of Chol reduced the leakage, since leakage values of 87% and 81% were found for lipid compositions of EPC/ESM/Chol at molar ratios of 5:3:1 and 5:1:1, respectively. When the Chol content was higher than ESM, leakage was much reduced (EPC/ESM/Chol at a molar ratio of 5:1:3 presented 37% of leakage). The inclusion of Chol but no ESM on EPC membranes reduced leakage, since EPC/Chol at molar ratios of 5:1 and 5:3 presented leakage values of 72% and 11%, respectively. Definitively Chol lowers the leakage elicited by the peptide, since its addition to different membrane compositions induced significant lower leakage values. We have studied the effect of the $NS4B_{AH2}$ peptide on membrane rupture using a complex lipid composition resembling the ER membrane to assess the effect of each component of the complex mixture (Fig. 2C). The synthetic ER complex membrane used above was composed of EPC, CL, BPI, TPE, BPS, EPA, ESM and Chol at a molar ratio of 59:0.37:7.4:18:3.1:1.2:3.4:7.8 [46]. Therefore we have designed an additional ER synthetic membrane composed of the same types of lipids, i.e., EPC/CL/BPI/TPE/BPS/EPA/ESM/Chol, but at a molar ratio of 58:6:6:6.6:6:6:6 ($ER^{58:6}$). As shown in Fig. 2C, $NS4B_{AH2}$ was capable of rupturing the $ER^{58:6}$ complex membrane: at a lipid/peptide ratio of 150:1 about 40% leakage was observed. In contrast, a leakage value of about 60% was obtained for the ER complex mixture at a lipid/peptide ratio of 150:1 (Fig. 2A). Leakage values were minor at higher lipid/peptide ratios. For example, at a lipid/peptide ratio of 800:1 no leakage was observed for the $ER^{58:6}$ complex membrane, but it was about 30% for the ER complex one. Removing either Chol or CL leakage values increased, whereas removing either ESM, BPS or TPE leakage values decreased (Fig. 2C). The removal of either EPA or BPI did not have any significant difference.

Since CF is a relatively small molecule (Stokes radius about 6 Å) we have studied the release of membrane-encapsulated bigger size molecules such as FITC–dextrans FD20 and FD70 (Stokes radius about 33 Å and 60 Å, respectively) [47,48]. In that way we could characterize the size of the pores which would be formed, if any, by the $NS4B_{AH2}$ peptide. As observed in Fig. 2D and E, $NS4B_{AH2}$ was capable of inducing a significant percentage of leakage for both FD20 and FD70 fluorophores, although at slightly slower different values than CF at comparable lipid/peptide ratios. For example, 80% CF leakage was observed for the ER complex mixture but 70% and 90% for FD20 and FD70 respectively. Lower values were observed for negatively-charged phospholipid containing compositions. For EPC/EPA and EPC/BPS at a molar ratio of 5:2 about 40% and 50% leakage values were observed for FD20 and FD70 but 80% for CF (Fig. 2A, D and E). Smaller values were observed for Chol containing liposomes. For CF, 80–90% leakage was observed (Fig. 2B) but 10–20% for FD20 (Fig. 2D) and about 30–60% for FD70 (Fig. 2E). The capacity of the $NS4B_{AH2}$ peptide to induce leakage of FITC–dextrans although to a lower extent than the small CF molecule demonstrates that $NS4B_{AH2}$ is capable of forming pores in the membrane [49], although rupture of the membrane at a later stage should not be ruled out.

The effect of the peptide on the structural and thermotropic properties of phospholipid membranes was investigated by measuring the steady-state fluorescence anisotropy of the fluorescent probes DPH and TMA-DPH incorporated into model membranes composed of different types of phospholipids as a function of temperature (Fig. 3). When DMPC was studied in the presence of the $NS4B_{AH2}$ peptide, there was a small change in the cooperativity of the thermal transition, as well as a small decrease in the T_m of DMPC when compared with the pure phospholipid (Fig. 3A and B). Additionally, the anisotropy of both DPH and TMA-DPH probes was slightly decreased and increased below and above the T_m, respectively. When the negatively charged phospholipids DMPG, DMPA, and DMPS were studied, $NS4B_{AH2}$ induced a decrease in the T_m of the main transition; this decrease was more noticeable for DMPG and DMPS than for DMPA (Fig. 3C, D, E, F, G and H). Similar to DMPC, the anisotropy of both DPH and TMA-DPH was slightly affected both below and above T_m. The effect of $NS4B_{AH2}$ on two phospholipids, namely PSM and 14BMP, was also studied (Fig. 3I, J, K and L). Similar to what was found above, the peptide decreased slightly the T_m and increased the anisotropy of DPH above but not below T_m. Three different binary mixtures were also studied, i.e., DMPC/DMPS at a molar ratio of 1:1 (Fig. 4M and N), DMPC/DMPA at a molar ratio of 1:1 (Fig. 3O and P), and DMPC/PSM at a molar ratio of 1:1 (Fig. 3Q and R). In all of the mixtures, $NS4B_{AH2}$ induced a decrease in the T_m of the main transition, being more noticeable in both DMPC/DMPS and DMPC/DMPA samples than in the DMPC/PSM one. Similar to what was found above, the anisotropy of both DPH and TMA-DPH above but not below the T_m was increased. $NS4B_{AH2}$ is therefore capable of affecting the thermal transition T_m of these phospholipids as observed by both types of probes; the peptide changed the anisotropy of DPH to a greater extent than TMA-DPH, so it should be located slightly deeper in the membrane, influencing the fluidity of the phospholipids [50].

The effect of the $NS4B_{AH2}$ peptide on the thermotropic phase behavior of phospholipid multilamellar vesicles was also studied using differential scanning calorimetry, DSC (Fig. 4). DMPC and DMPG display two endothermic peaks on heating, the pre-transition (appearing at about 12–14 °C, $L_{\beta'}$–$P_{\beta'}$) and the main transition (appearing at about 23–24 °C, $P_{\beta'}$–L_α). Incorporation of $NS4B_{AH2}$ in DMPC at a lipid/peptide ratio of 15:1 (Fig. 4A), did not significantly alter the thermotropic behavior of the phospholipid, since the peptide did not completely abolish the pre-transition; the main transition of DMPC was slightly broadened and shifted to lower temperatures than the T_m. When $NS4B_{AH2}$ was incorporated into DMPG at the same lipid/peptide ratio, the pre-transition waned, and the main transition broadened significantly giving rise to two different peaks, which should be due to mixed phases (Fig. 4B). DMPS and DMPA present a single highly cooperative phase transition that corresponds to the chain melting transition from the gel to the liquid-crystalline phases [51]. The presence of $NS4B_{AH2}$ at a lipid/peptide molar ratio of 15:1 induced a slight decrease of cooperativity in DMPS as well as a shift to lower temperatures of the main phase transition of the phospholipid (Fig. 4C). In the case of DMPA, $NS4B_{Cter}$ induced a slight shift to higher temperatures of the main phase transition peak of the phospholipid but no decrease in cooperativity was observed (Fig. 4D). DEPE presents two transitions, a gel to liquid-crystalline phase transition (L_β–L_α) in the lamellar phase at about 38 °C and in addition a lamellar liquid-crystalline to hexagonal-H_{II} (L_α–H_{II}) phase transition at about 63 °C [52]. $NS4B_{AH2}$ did not induce any effect on the main transition of the lipid but decreased the cooperativity of the lamellar to hexagonal phase transition (Fig. 4E). As observed in Fig. 4F, 14BMP displays two endothermic peaks on heating, a small transition at about 19 °C from a quasi-crystalline phase L_{c1} to a quasi-crystalline phase with different tilt angle L_{c2} and a main transition at about 41 °C from a quasi-crystalline phase L_{c2} to the liquid phase L_α [53]. The incorporation of $NS4B_{AH2}$ into 14BMP membranes at a lipid/peptide ratio of 15:1 did not alter the thermotropic behavior of the phospholipid, since no significant effect was observed on the two transitions of 14BMP (Fig. 4F). PSM presents a single highly cooperative phase transition at about 41 °C corresponding to the gel-to-liquid-crystalline phase main transition. The incorporation of $NS4B_{AH2}$ into PSM membranes altered the thermotropic behavior of the phospholipid, inducing a broadening of the main transition peak (Fig. 4E).

Since the ^{31}P NMR isotropic chemical shifts of both ESM and EPC head-group peaks are resolvable under MAS conditions we have used ^{31}P MAS NMR to observe EPC, ESM and Chol containing mixtures in the presence of the $NS4B_{AH2}$ peptide. When the mixtures EPC/ESM at a molar ratio of 5:3 and EPC/ESM/Chol at a molar ratio of 5:3:3 were studied, they presented two bands corresponding to EPC and

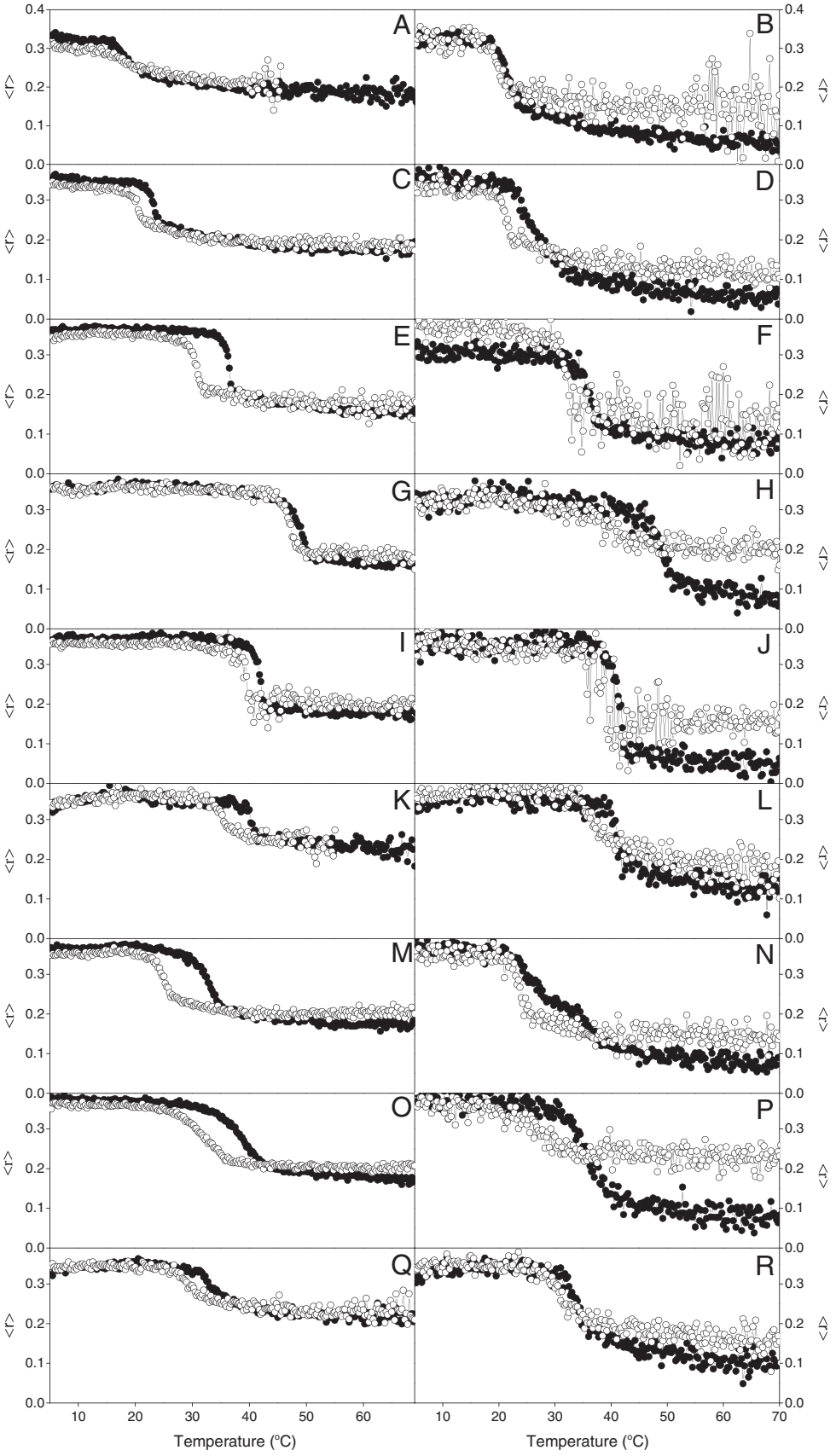

Fig. 3. Steady-state anisotropy, <r>, of TMA-DPH (A, C, E, G, I, K, M, O, Q) and DPH (B, D, F, H, J, L, N, P, R) incorporated into (A, B) DMPC, (C, D) DMPG, (E, F) DMPS, (G, H) DMPA, (I, J) 14BMP, (K, L) PSM, (M, N) DMPS/DMPC at a molar ratio of 1:1, (O,P) DMPA/DMPC at a molar ratio of 1:1 and (Q,R) PSM/DMPC at a molar ratio of 1:1 model membranes as a function of temperature. Data correspond to vesicles containing pure phospholipids (●) and phospholipids plus $NS4B_{AH2}$ peptide (○). The peptide to phospholipid molar ratio was 1:15.

ESM with an individual intensity reflecting its composition (Fig. 5). The chemical shift of both EPC and ESM resonances was not significantly different neither in the absence nor in the presence of $NS4B_{AH2}$, but the line widths of the ^{31}P resonances of EPC and ESM were significantly increased in the presence of the peptide. The width of the EPC and ESM peaks in the EPC/ESM mixture in the absence of the peptide was 48 and 47 Hz, respectively; in the presence of the peptide, the width of the EPC and ESM peaks increased to 86

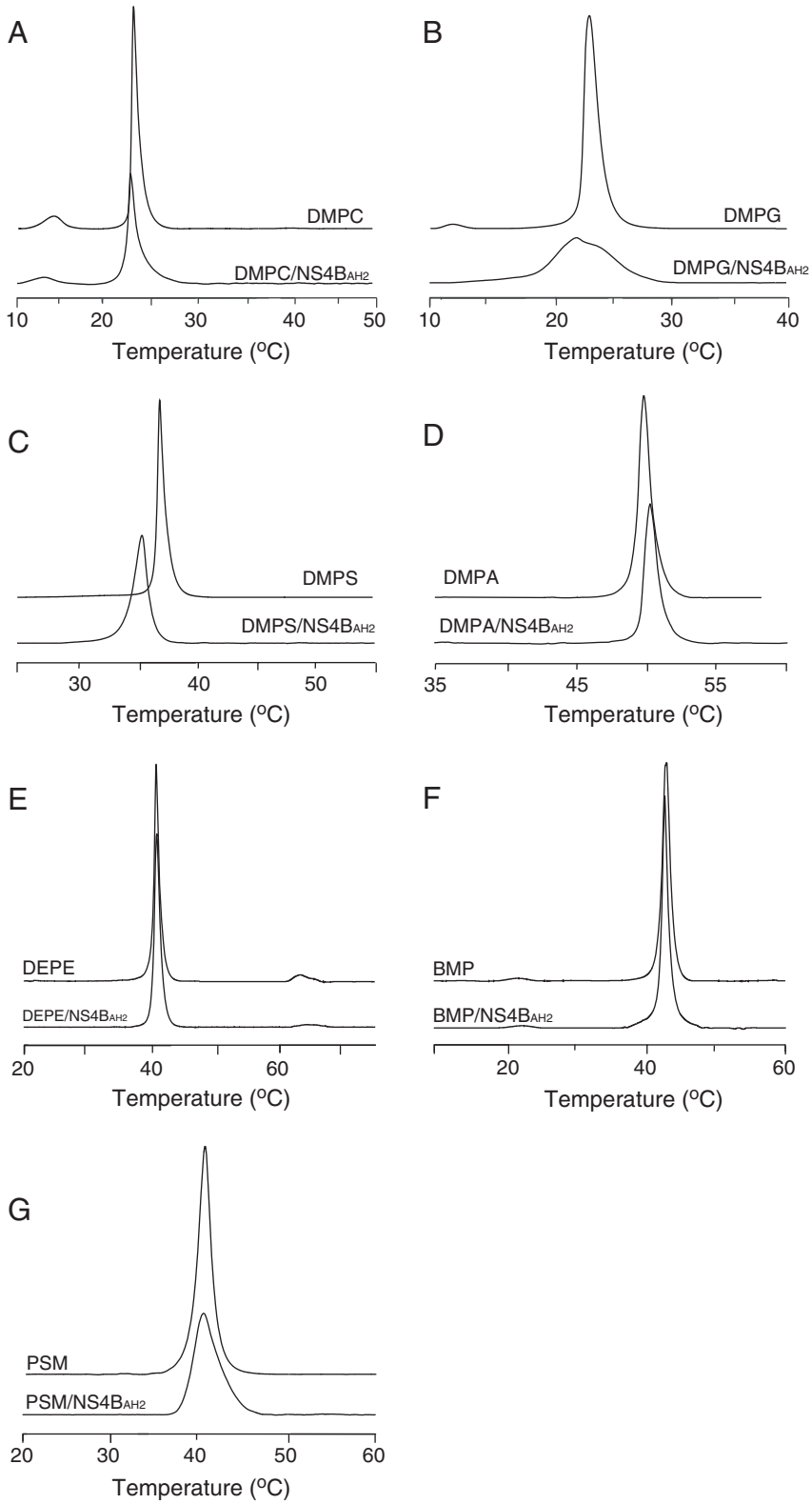

Fig. 4. Differential scanning calorimetry heating-scan thermograms for model membranes composed of (A) DMPC, (B) DMPG, (C) DMPS, (D) DMPA, (E) DEPE, (F) 14BMP and (G) PSM in the absence (upper thermogram) and in the presence (lower thermogram) of the $NS4B_{AH2}$ peptide. The peptide to phospholipid molar ratio was 1:15. All thermograms were normalized to the same amount of lipid.

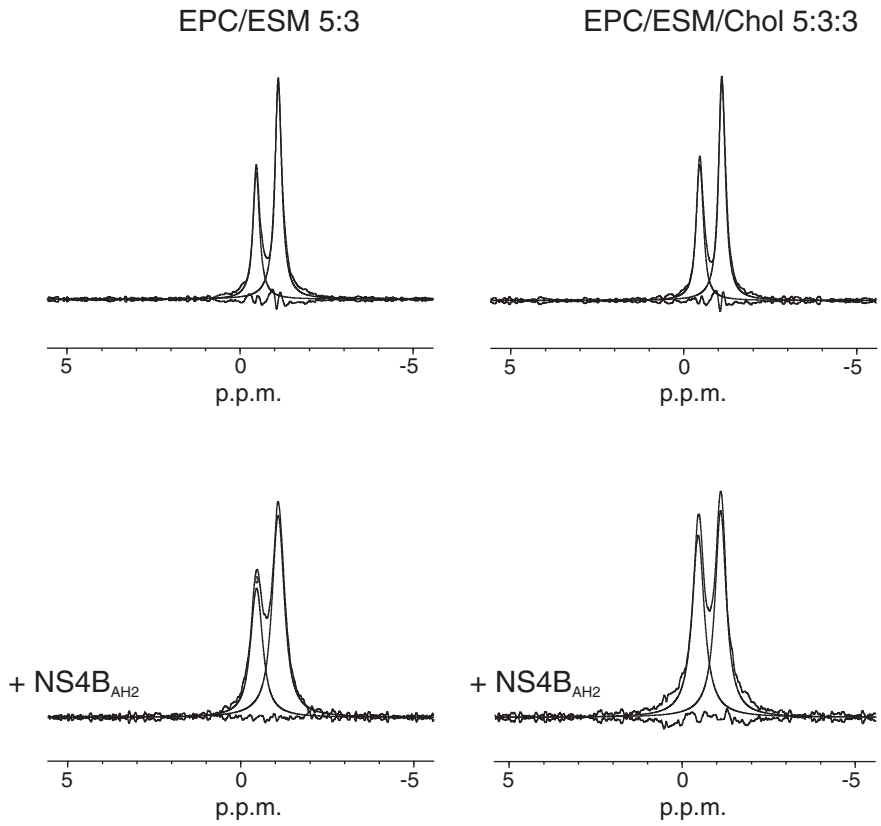

Fig. 5. MAS ^{31}P-NMR spectra at 20 °C and 8 kHz spinning speed (500 MHz proton frequency) for multilamellar suspensions of EPC/ESM at a molar ratio of 5:3 and EPC/ESM/Chol at a molar ratio of 5:3:3 in the presence of peptide NS4B$_{AH2}$ at a phospholipid/peptide molar ratio of 15:1. The original spectra, the fitted bands and the differences are shown.

and 85 Hz. The width of the EPC and ESM peaks in the EPC/ESM/Chol mixture and in the absence of the peptide was 48 and 51 Hz, respectively; however, the width of the EPC and ESM peaks was 79 and 86 Hz, respectively, when NS4B$_{AH2}$ was present. The presence of the NS4B$_{AH2}$ peptide induced a similar increase in the width of both EPC and ESM peaks in the complex mixtures, indicating no specific interaction for both types of phospholipids. However, it is interesting to note that the increase in bandwidth induced by the peptide is smaller for the EPC/ESM/Chol sample than for the EPC/ESM one. The increase in bandwidth for EPC and ESM in the EPC/ESM sample was 38 Hz whereas the increase in bandwidth for EPC and ESM in the EPC/ESM/Chol sample was 31 and 35 Hz, respectively. These data would be in accordance with the fluorescence and leakage data shown above, since Chol reduces the interaction of the peptide with the membrane.

We have analyzed the infrared Amide I′ band of the NS4B$_{AH2}$ peptide located between 1700 and 1600 cm^{-1} in the presence of different membrane model systems (Fig. 6). For the peptide in solution, the broad Amide I′ band was asymmetric and displayed bands at different frequencies with different intensities (Fig. 6E). At low temperatures, a relatively narrow band at about 1621 cm^{-1} was apparent with a shoulder at about 1645 cm^{-1} and a small peak at about 1681 cm^{-1}. At higher temperatures, the band at 1621 cm^{-1} shifted to about 1623 cm^{-1}, the band at about 1645 cm^{-1} disappeared and a new band at about 1656 cm^{-1} appeared, albeit with lower intensity. The small peak at about 1681 cm^{-1} did not change in frequency (Fig. 6E). The appearance of a band at approximately 1618–1622 cm^{-1} concomitantly with another one at about 1680 cm^{-1} would indicate the existence of aggregated β structures, whereas the broad band with the intensity maxima at about 1645 cm^{-1} would correspond to a mixture of unordered and helical structures, and the band at about 1645 cm^{-1} would mainly correspond to helical structures [54,55]. The NS4B$_{AH2}$ peptide would then change from a mixture of helical, unordered and aggregated β structures at low temperatures to a mixture of helical and aggregated β structures at high temperatures, this transitional change in overall structure occurring steadily from low to high temperatures (Fig. 6E). In the presence of DMPC the Amide I′ envelope of the NS4B$_{Cter}$ peptide presented a broad band with a maximum at about 1623 cm^{-1} at all temperatures. The spectrum envelope would suggest that, although helical and unordered structures might be present, the main secondary structure component consists of aggregated structures (Fig. 6F). In the presence of either DMPG, DMPA or BMP and at all temperatures, the Amide I′ envelope of NS4B$_{AH2}$ was rather similar. In this case, the broad band was asymmetric, with a maximum at about 1624 cm^{-1} and a shoulder at about 1655 cm^{-1} (Fig. 6G, H and I). These data would suggest that the main secondary structure component should be aggregated structures although helical structures might be present; the peptide would present a high degree of conformational stability in the presence of phospholipids.

We have also analyzed the ester C═O band of the phospholipids located between 1745 and 1720 cm^{-1} in the presence of the NS4B$_{AH2}$ peptide (Fig. 6). The frequency maximum of the ester C═O band of DMPC displayed one transition at about 24 °C, coincident with the main gel to liquid crystalline phase transition of the pure phospholipid (Fig. 6A and J). In the presence of NS4B$_{AH2}$, the frequency of the ester C═O band of DMPC displayed only one transition at about 24 °C, in accordance with the DSC data (see Fig. 4A). However, its absolute frequency was higher in the presence of the peptide than in its absence, suggesting that the peptide increased the intensity of the 1743 cm^{-1} component relative to the 1727 cm^{-1} one, i.e., the amount of non-hydrogen bonded C═O ester bands increased in the presence of the peptide [56,57]. The pattern of the thermotropic phase behavior exhibited by pure DMPG is similar to that of pure

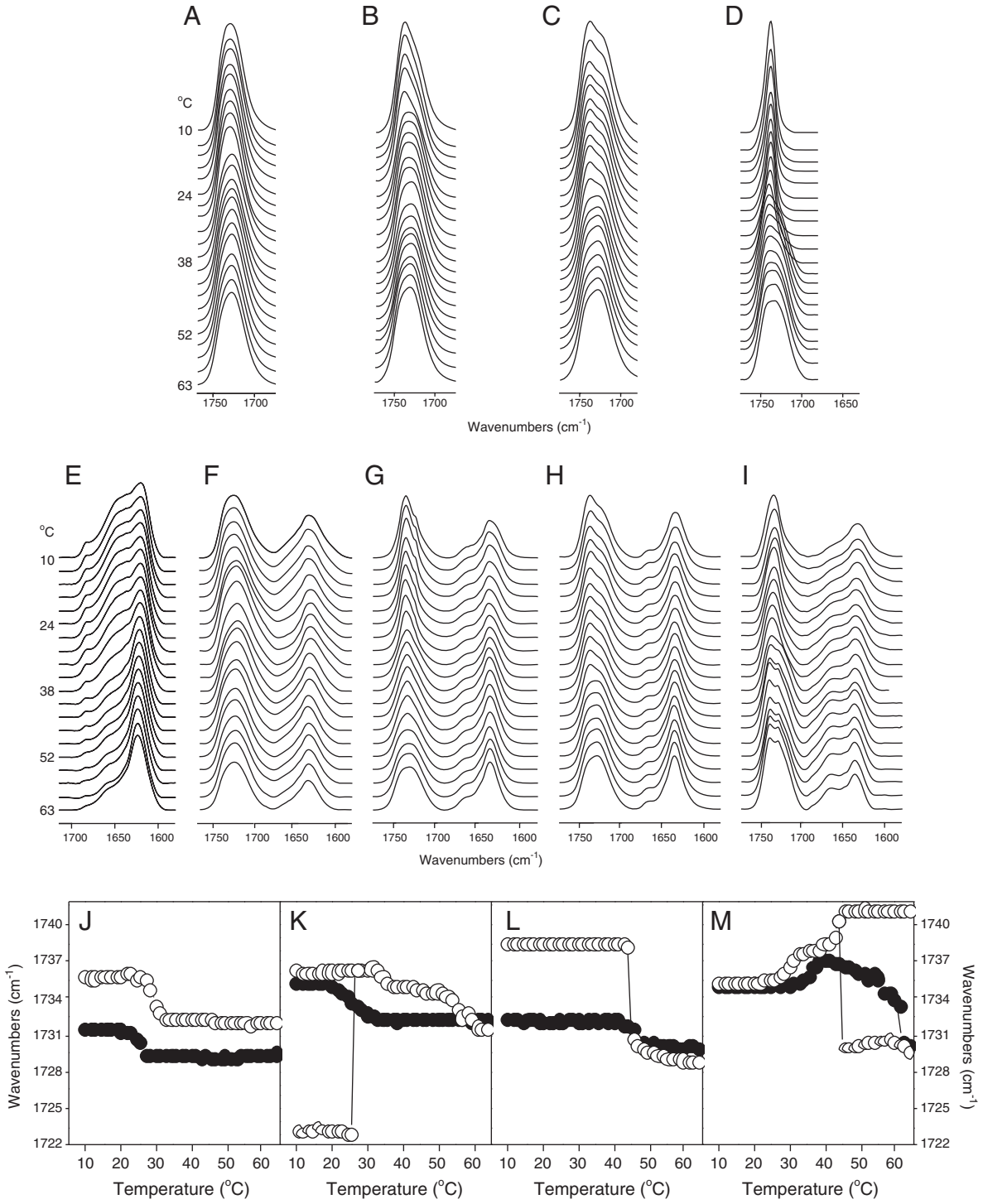

Fig. 6. Stacked infrared spectra of the C═O region of pure (A) DMPC, (B) DMPG, (C) DMPA and (D) 14BMP and the C═O and Amide I′ regions for the NS4B$_{AH2}$ peptide in solution (E) and in the presence of (F) DMPC, (G) DMPG, (H) DMPA and (I) 14BMP at different temperatures as indicated. The temperature dependence of the C═O carbonyl stretching band frequencies for (J) DMPC, (K) DMPG, (L) DMPA and (M) 14BMP in the absence (●) and in the presence (○) of the NS4B$_{AH2}$ peptide. The phospholipid/peptide molar ratio was 15:1.

DMPC (Fig. 6B and K). However, in the presence of the peptide and at low temperatures, the C═O carbonyl band of DMPC presented a main peak and a shoulder, which could suggest the formation of a quasi-crystalline lamellar phase [58,59]. At higher temperatures the two peaks coalesced into a broad C═O band similar in appearance to the one observed for pure DMPG, suggesting the formation of a normal liquid crystalline phase (Fig. 6B and K). The ester C═O band of DMPA displayed a single transition in accordance with the DSC data (Fig. 6C and L). In the presence of NS4B$_{AH2}$ only one transition was observed but the frequency of the C═O band at low temperatures appeared at about 1738 cm^{-1} indicating, as above, that the amount of free, i.e., non-hydrogen, bonded C═O ester bands increased in the presence of the peptide. At temperatures above the main transition the frequencies in the absence and in the presence of the peptide were similar (Fig. 6L). The ester C═O band of pure 14BMP displayed a sharp band at low temperatures and a broad one at high temperatures, defining the transition temperature of the phospholipid (Fig. 6D and M). In the presence of NS4B$_{AH2}$, the ester

C═O band of 14BMP displayed a transition at about 30 °C and another one at about 45 °C. In this last case, the C═O band was formed by two sharp peaks and a shoulder.

In order to investigate the possible lipid binding specificity of the $NS4B_{AH2}$ peptide a peptide–lipid overlay assay was performed using different nitrocellulose membrane strips with different lipids and concentrations (Fig. 7). As stated in the Materials and methods section, a penta-His derived peptide from $NS4B_{AH2}$ was used, $NS4B_{AH2\text{-}His}$, in addition to a scrambled version, $NS4B_{SCAH2\text{-}His}$. As shown in Fig. 7A, $NS4B_{AH2\text{-}His}$ was capable of binding with high affinity to different phosphatidyl inositol phosphates, namely phosphatidylinositol-4-phosphate, phosphatidylinositol-4,5-bisphosphate and phosphatidylinositol-3,4,5-trisphosphate; however, the binding of the scrambled derivative was not as remarkable. Array strips with increasing amount of phosphatidylinositol phosphates per spot were also used, showing that $NS4B_{AH2\text{-}His}$ was capable of binding strongly to several phosphatidylinositol-phosphates, mainly phosphatidylinositol-4-phosphate and phosphatidylinositol-5-phosphate (Fig. 7B). $NS4B_{AH2\text{-}His}$ was also capable of binding weakly to other phosphatidyl inositol phosphates but only at the highest lipid concentrations used in the assay (Fig. 7B). The lipids on the nitrocellulose membrane strips do not imitate the real biological membrane structure but give a qualitative answer to binding of the peptide to certain phospholipids. Nonetheless, the $NS4B_{AH2\text{-}His}$ peptide was able of binding to several phosphatidyl inositol phosphates in a specific way but no other lipids.

Given the capability of the $NS4B_{AH2}$ peptide to disrupt and absorb into membranes, we were interested in visualizing the effect of the peptide on the topography and stability of phase separated zwitterionic planar lipid bilayers. AFM was used for this purpose. In this work, lipid bilayers composed of POPC/DPPC at a molar ratio of 1:1, POPC/PSM at a molar ratio of 5:3, DOPC/PSM/Chol at a molar ratio of 5:3:2 and DOPC/DSPC/Chol at a molar ratio of 2:2:1 were imaged before and after incubation with $NS4B_{AH2}$ at 0.5 μM, 1 μM and 3 μM (Fig. 8). The peptide induced significant changes on POPC/DPPC and POPC/PSM membrane topography but did not cause any significant changes on DOPC/DSPC/Chol membranes (Fig. 8). In the case of DOPC/PSM/Chol membrane systems, upon addition of peptide at a concentration of 1 μM and after 30 min incubation, slight defects and small aggregates over the membrane surface were observed. Upon addition of peptide at 3 μM to membrane systems with Chol, too many aggregates were observed (image not shown). Upon addition of the peptide at a concentration of 1 μM to POPC/DPPC and POPC/PSM membrane systems, small perturbations of the gel matrix borders were observed. In addition, the peptide at 3 μM causes significant changes in the gel and fluid matrix for POPC/DPPC and for POPC/PSM, being the effect more pronounced at the gel matrix borders.

4. Discussion

Most, if not all, of the HCV non-structural proteins including NS4B, play a central role in viral particle formation and budding, but their specific function in replication and/or assembly remains poorly understood [6,60]. HCV NS4B is a highly hydrophobic protein that has been suggested to alter intracellular host membranes making possible the formation of the HCV replication complex, playing a critical role in the HCV life cycle. NS4B is a multifunctional membrane protein that possesses different regions where diverse and significant functions are located. One of these important regions is the AH2 segment,

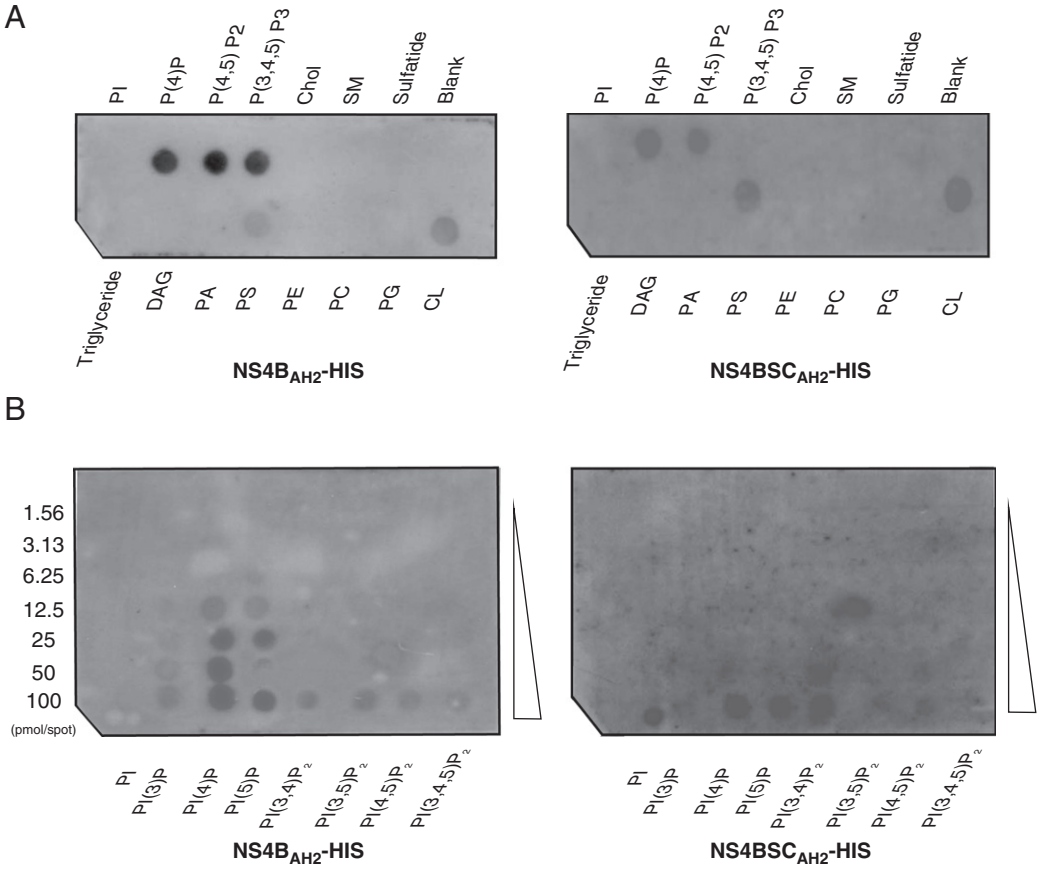

Fig. 7. $NS4B_{AH2}$ peptide-lipid overlay binding assay. (A) Assay for triglyceride, diacylglycerol (DAG), phosphatidic acid (PA), phosphatidylserine (PS), phosphatidylethanolamine (PE), phosphatidylcholine (PC), phosphatidylglycerol (PG), cardiolipin (CL), phosphatidylinositol (PI), phosphatidylinositol-4-phosphate (PI(4)P), phosphatidylinositol-4,5-bisphosphate, ($PI(4,5)P_2$), phosphatidylinositol-3,4,5-trisphosphate ($PI(3,4,5)P_3$), cholesterol (Chol), sphingomyelin (SM), and 3-sulfogalactosylceramide (sulfatide). Each spot contains 100 pmol of each one of the lipids. (B) Concentration array of phosphatidylinositol (PI), phosphatidylinositol-4-phosphate (PI(4)P), phosphatidylinositol-4,5-bisphosphate, ($PI(4,5)P_2$), phosphatidylinositol-3,4,5-trisphosphate ($PI(3,4,5)P_3$). The strips shown in the figure are from one representative experiment out of three. See text for further details.

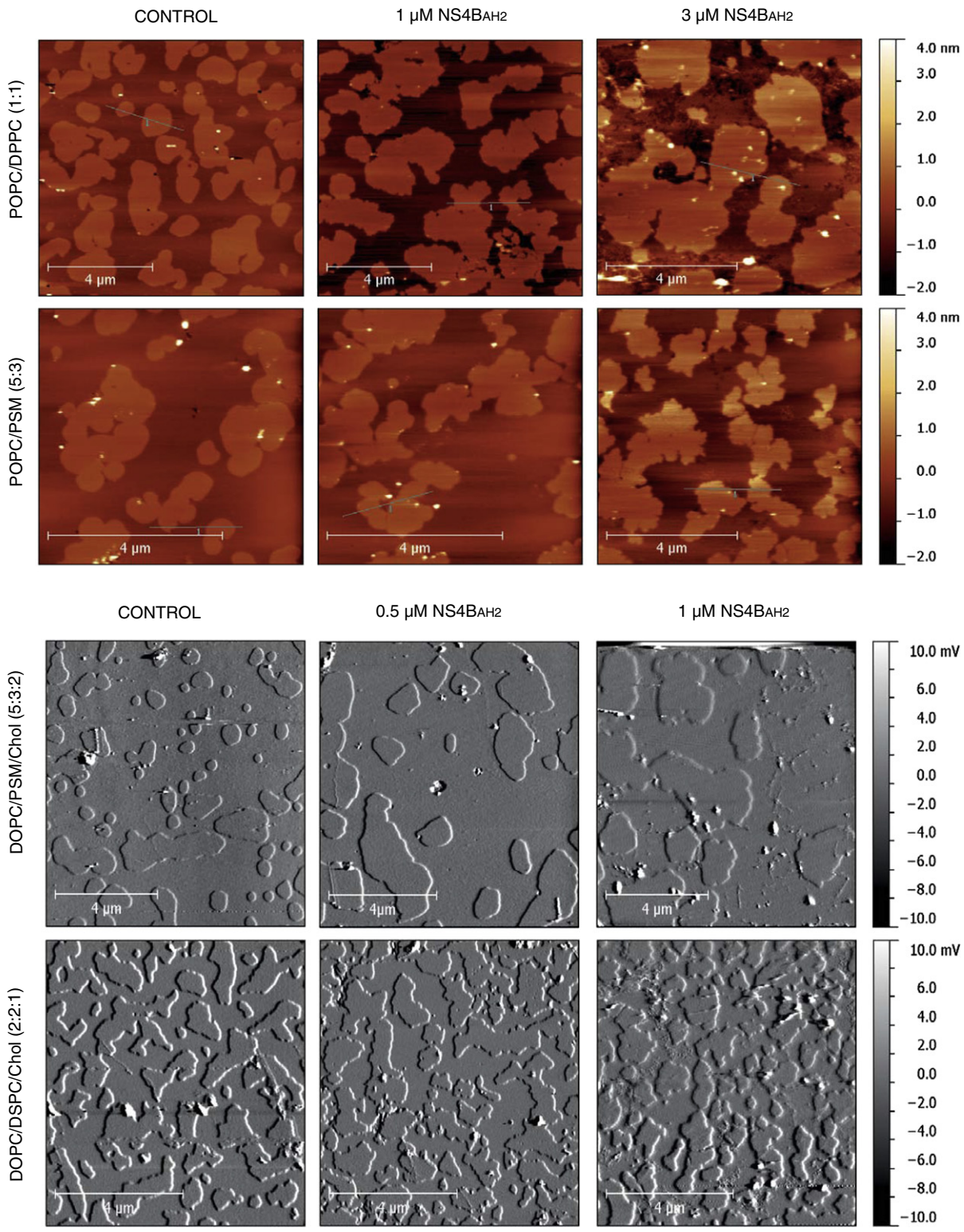

Fig. 8. Effect of $NS4B_{AH2}$ on the topography of zwitterionic supported lipid bilayers. AFM height images of POPC/DPPC (1:1) and POPC/PSM (5:3) supported lipid bilayers, and AFM error images of DOPC/DSPC/Chol (2:2:1) and DOPC/PSM/Chol (5:3:2) bilayers are shown in the presence of $NS4B_{AH2}$ peptide at 0.5 μM, 1 μM and 3 μM. Control measurements were performed in the absence of peptide.

which besides being highly conserved has been shown to play a significant role in NS4B functioning [13,17]. Since the biological role/roles of NS4B is/are intrinsically related to the membrane, we have extended our previous works to investigate the binding and interaction of this highly conserved membranotropic AH2 region of NS4B, i.e., peptide $NS4B_{AH2}$, with different membrane model systems. We have carried out an in-depth biophysical study aimed at the elucidation of the capacity of this region to interact and disrupt membranes, as well as to study the structural and dynamic features which might be relevant for that disruption. Our findings give interesting clues to

a key region in the NS4B protein that might be implicated in the HCV life cycle.

We have shown that the $NS4B_{AH2}$ peptide binds with high affinity to phospholipid model membranes, as it has been found for other peptides [44,61]. Hydrophilic quenching probes further demonstrated binding of the peptide to the membrane, since the $NS4B_{AH2}$ peptide was less accessible for quenching by acrylamide implying a buried location. The lipophilic probe quenching results suggest a shallow-to-intermediate location of the peptide in the membrane. Interestingly, these data suggest that the insertion of the peptide into the bilayer palisade depends on phospholipid composition. We have also shown that the $NS4B_{AH2}$ peptide is capable of affecting the steady state fluorescence anisotropy of fluorescent probes located into the palisade structure of the membrane, since the peptide was able of decreasing the mobility and cooperativity of the phospholipid acyl chains when compared to the pure phospholipids. Calorimetry experiments indicated that the $NS4B_{AH2}$ peptide induced the presence of mixed lipid phases, enriched and impoverished in peptide. These results suggest that the location of the peptide is at or near the membrane interface, influencing the fluidity of the phospholipids, most probably with an in-plane orientation rather than in a transmembrane position [62]. This location would be in accordance with previous data obtained for the two proposed α-helical elements of the C-terminal region [16,33]. Interestingly, $NS4B_{AH2}$ is capable of binding different phosphatidyl inositol phosphates with high affinity, implying that this NS4B segment could be implicated in either the recruitment of phosphatidyl inositol phosphates in the replication complex or specific domain formation or both [63]. Moreover, its interfacial properties suggest that this segment could behave similarly to a pre-transmembrane domain partitioning into and interacting with the membrane depending on the membrane composition and/or other proteins [36,64,65], being the responsible of the fluctuation of the protein between different topologies and therefore possible locations [8,9,66].

The $NS4B_{AH2}$ peptide was also capable of altering membrane stability causing the release of fluorescent probes through pores in the membrane. The release of these probes was dependent on both the lipid/peptide molar ratio and lipid composition. The formation of pores would imply a possible oligomerization of the peptide, which would substantiate the possible role of this NS4B segment in protein-protein oligomerization [13]. Apart from that, the binding of AH2 to specific phospholipids in the membrane as demonstrated in this work could also promote protein oligomerization through the formation of lipid domains in the membrane. The highest CF release was observed for liposomes containing the phospholipid BMP, although significant leakage values were also observed for liposomes composed of both zwitterionic and negatively-charged phospholipids. Significantly, at a lipid to peptide molar ratio as high as 800 to 1, a leakage value of 100% was observed for BMP membranes. Interestingly, Chol seems to lower the leakage elicited by the peptide, since its addition to different membrane compositions induced lower leakage values. The differential effect observed when Chol was included in the membrane was also supported by the AFM data. These differences could be a consequence of influence of cholesterol in the membrane penetration of peptides preventing its insertion as it has been observed for other peptides [67]. As a general trend, it can be observed that the higher the ESM content and the lower the Chol content, the higher the leakage values are. These results were corroborated by using a specific ER complex membrane, indicating that the specific disrupting effect elicited by the $NS4B_{AH2}$ peptide should depend on the phospholipid head-group characteristics, i.e., charge and possibly hydrogen bonding, although hydrophobic interactions within the bilayer should not be ruled out. The ^{31}P MAS NMR results show that both phospholipids, EPC and ESM, exhibit a lower degree of mobility in the presence of the peptide [68]. Taking into account all these data, the specific disrupting effect elicited by $NS4B_{AH2}$ should be primarily due to hydrophobic interactions within the bilayer, although the specific charge of the phospholipid head-groups affects, slightly, the extent of membrane leakage.

The infrared spectra of the Amide I′ region of the fully hydrated $NS4B_{AH2}$ peptide in solution at low temperatures displayed a coexistence of unordered, aggregated and helical structures, which at high temperatures became a mixture of helical and aggregated structures. In the presence of different phospholipids as well as at different temperatures, the main secondary structure component was mainly aggregated structure. These results imply that the secondary structure of the $NS4B_{AH2}$ peptide was affected by its binding to the membrane, so that membrane binding modulates the secondary structure of the peptide as it has been suggested for other peptides [31,33]. In the presence of membranes, the overall secondary structure of the peptide did not change, demonstrating a high stable conformation in the bound state. At the same time, differences in the frequency and number of bands corresponding to the carbonyl band of the phospholipids were observed, showing that peptide binding also modulated phospholipid conformation.

The NS4B region where peptide $NS4B_{AH2}$ resides might have an essential role in the membrane replication and/or assembly of the viral particle through the modulation of the membrane structure and hence the replication complex. The conservation of its structure as well as its physical and chemical properties should be essential in

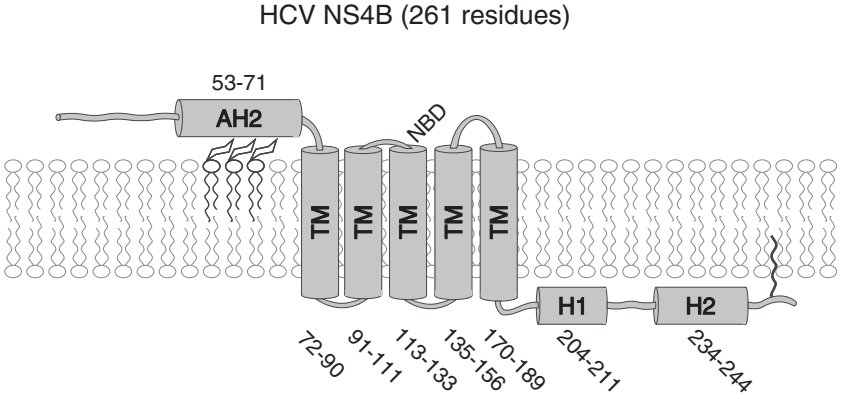

Fig. 9. Schematic representation of protein NS4B from HCV. The N-terminal region of the protein contains the amphipathic segment AH2, whereas the C-terminal part contains two α-helical segments, H1 and H2. In between these two regions, five transmembrane (TM) segments can be found. As shown in this work, AH2 would be capable of binding specific phospholipids such as PIPs. NS4B contains a nucleotide binding domain (NBD) as well as a palmitoylation site, as indicated. Residue numbers show the approximate extension of the different segments [10]. The protein segments have been roughly drawn to scale.

its function. Our results add new information about how this region can contribute to the interaction with the membrane. Although the peptide is not deeply buried in the membrane, its interaction with the membrane depends on its composition and it is able to affect the lipid milieu from the membrane surface down to the hydrophobic core. The existence of a number of hydrophobic and interfacial regions in HCV NS4B protein would suggest that they could oscillate between metastable and stable conformations; moreover, their different biological functions would define the mechanism of the viral replication complex formation. We have shown previously that NS4B possesses five transmembrane segments [10] flanked by the N- and C-terminal regions where segments AH2 and H1/H2 are located [13,15,16,33] (Fig. 9). Whereas the integral part of the protein, showing ATP/GTPase activity, localizes it in the membrane, the N- and C-terminal regions modulate membrane structure, bind specific phospholipids and are responsible of homo and/or hetero-oligomerization. NS4B, a multifunctional integral membrane protein with several segments having defined biological functions, essential for the formation of the replication complex, would therefore have a dynamic membrane topology which would be inherent to its biological functioning. These conformational changes could be envisaged as driven by the interaction with specific lipids or domains in the membrane or even proteins. Consequently, the results described in this work identify an important region in the HCV NS4B protein, which might be of critical importance in the HCV life cycle. Additionally, pharmacological disruption of NS4B interaction with membranes could represent the basis for a novel approach to anti-HCV therapy.

Acknowledgements

This work was partially supported by grants REEQ/140/BIO/2005, PTDC/QUI-BIQ/114774/2009 and PTDC/QUI-BIQ/112929/2009 to M.R.B.C (FCT-MES, Portugal). H.N. is supported by a “Santiago Grisolía” fellowship from Generalitat Valenciana Autonomous Government, Spain. F.P.J. acknowledges FEBS for a Short Term Fellowship.

References

[1] C.W. Shepard, L. Finelli, M.J. Alter, Global epidemiology of hepatitis C virus infection, Lancet Infect. Dis. 5 (2005) 558–567.
[2] S.A. Sarbah, Z.M. Younossi, Hepatitis C: an update on the silent epidemic, J. Clin. Gastroenterol. 30 (2000) 125–143.
[3] Global surveillance and control of hepatitis C. Report of a WHO Consultation organized in collaboration with the Viral Hepatitis Prevention Board, Antwerp, Belgium, J. Viral Hepat. 6 (1999) 35–47.
[4] C. Vauloup-Fellous, V. Pene, J. Garaud-Aunis, F. Harper, S. Bardin, Y. Suire, E. Pichard, A. Schmitt, P. Sogni, G. Pierron, P. Briand, A.R. Rosenberg, Signal peptide peptidase-catalyzed cleavage of hepatitis C virus core protein is dispensable for virus budding but destabilizes the viral capsid, J. Biol. Chem. 281 (2006) 27679–27692.
[5] H. Tang, H. Grise, Cellular and molecular biology of HCV infection and hepatitis, Clin. Sci. (Lond.) 117 (2009) 49–65.
[6] D. Moradpour, F. Penin, C.M. Rice, Replication of hepatitis C virus, Nat. Rev. Microbiol. 5 (2007) 453–463.
[7] J. McLauchlan, Lipid droplets and hepatitis C virus infection, Biochim. Biophys. Acta 1791 (2009) 552–559.
[8] T. Hugle, F. Fehrmann, E. Bieck, M. Kohara, H.G. Krausslich, C.M. Rice, H.E. Blum, D. Moradpour, The hepatitis C virus nonstructural protein 4B is an integral endoplasmic reticulum membrane protein, Virology 284 (2001) 70–81.
[9] D. Egger, B. Wolk, R. Gosert, L. Bianchi, H.E. Blum, D. Moradpour, K. Bienz, Expression of hepatitis C virus proteins induces distinct membrane alterations including a candidate viral replication complex, J. Virol. 76 (2002) 5974–5984.
[10] F. Palomares-Jerez, H. Nemesio, J. Villalain, The membrane spanning domains of protein NS4B from hepatitis C virus, Biochim. Biophys. Acta 1818 (2012) 2958–2966.
[11] S. Einav, M. Elazar, T. Danieli, J.S. Glenn, A nucleotide binding motif in hepatitis C virus (HCV) NS4B mediates HCV RNA replication, J. Virol. 78 (2004) 11288–11295.
[12] S. Einav, E.H. Sklan, H.M. Moon, E. Gehrig, P. Liu, Y. Hao, A.W. Lowe, J.S. Glenn, The nucleotide binding motif of hepatitis C virus NS4B can mediate cellular transformation and tumor formation without Ha-ras co-transfection, Hepatology 47 (2008) 827–835.
[13] J. Gouttenoire, P. Roingeard, F. Penin, D. Moradpour, Amphipathic alpha-helix AH2 is a major determinant for the oligomerization of hepatitis C virus nonstructural protein 4B, J. Virol. 84 (2010) 12529–12537.
[14] D. Paul, I. Romero-Brey, J. Gouttenoire, S. Stoitsova, J. Krijnse-Locker, D. Moradpour, R. Bartenschlager, NS4B self-interaction through conserved C-terminal elements is required for the establishment of functional hepatitis C virus replication complexes, J. Virol. 85 (2011) 6963–6976.
[15] M.F. Palomares-Jerez, H. Nemesio, J. Villalain, Interaction with membranes of the full C-terminal domain of protein NS4B from hepatitis C virus, Biochim. Biophys. Acta 1818 (2012) 2536–2549.
[16] M.F. Palomares-Jerez, J. Villalain, Membrane interaction of segment H1 (NS4B(H1)) from hepatitis C virus non-structural protein 4B, Biochim. Biophys. Acta 1808 (2011) 1219–1229.
[17] J. Gouttenoire, V. Castet, R. Montserret, N. Arora, V. Raussens, J.M. Ruysschaert, E. Diesis, H.E. Blum, F. Penin, D. Moradpour, Identification of a novel determinant for membrane association in hepatitis C virus nonstructural protein 4B, J. Virol. 83 (2009) 6257–6268.
[18] H. Aizaki, K.J. Lee, V.M. Sung, H. Ishiko, M.M. Lai, Characterization of the hepatitis C virus RNA replication complex associated with lipid rafts, Virology 324 (2004) 450–461.
[19] J. Guillen, A. Gonzalez-Alvarez, J. Villalain, A membranotropic region in the C-terminal domain of hepatitis C virus protein NS4B interaction with membranes, Biochim. Biophys. Acta 1798 (2010) 327–337.
[20] A.J. Perez-Berna, M.R. Moreno, J. Guillen, A. Bernabeu, J. Villalain, The membrane-active regions of the hepatitis C virus E1 and E2 envelope glycoproteins, Biochemistry 45 (2006) 3755–3768.
[21] H. Nemesio, F. Palomares-Jerez, J. Villalain, NS4A and NS4B proteins from dengue virus: membranotropic regions, Biochim. Biophys. Acta 1818 (2012) 2818–2830.
[22] H. Nemesio, F. Palomares-Jerez, J. Villalain, The membrane-active regions of the dengue virus proteins C and E, Biochim. Biophys. Acta 1808 (2011) 2390–2402.
[23] M.R. Moreno, M. Giudici, J. Villalain, The membranotropic regions of the endo and ecto domains of HIV gp41 envelope glycoprotein, Biochim. Biophys. Acta 1758 (2006) 111–123.
[24] W.K. Surewicz, H.H. Mantsch, D. Chapman, Determination of protein secondary structure by Fourier transform infrared spectroscopy: a critical assessment, Biochemistry 32 (1993) 389–394.
[25] Y.P. Zhang, R.N. Lewis, R.S. Hodges, R.N. McElhaney, FTIR spectroscopic studies of the conformation and amide hydrogen exchange of a peptide model of the hydrophobic transmembrane alpha-helices of membrane proteins, Biochemistry 31 (1992) 11572–11578.
[26] L.D. Mayer, M.J. Hope, P.R. Cullis, Vesicles of variable sizes produced by a rapid extrusion procedure, Biochim. Biophys. Acta 858 (1986) 161–168.
[27] C.S.F. Böttcher, C.M. Van Gent, C. Fries, A rapid and sensitive sub-micro phosphorus determination, Anal. Chim. Acta 1061 (1961) 203–204.
[28] H. Edelhoch, Spectroscopic determination of tryptophan and tyrosine in proteins, Biochemistry 6 (1967) 1948–1954.
[29] M.R. Eftink, C.A. Ghiron, Exposure of tryptophanyl residues and protein dynamics, Biochemistry 16 (1977) 5546–5551.
[30] M.R. Moreno, J. Guillen, A.J. Perez-Berna, D. Amoros, A.I. Gomez, A. Bernabeu, J. Villalain, Characterization of the interaction of two peptides from the N terminus of the NHR domain of HIV-1 gp41 with phospholipid membranes, Biochemistry 46 (2007) 10572–10584.
[31] M.F. Palomares-Jerez, J. Guillen, J. Villalain, Interaction of the N-terminal segment of HCV protein NS5A with model membranes, Biochim. Biophys. Acta 1798 (2010) 1212–1224.
[32] A. Bernabeu, J. Guillen, A.J. Perez-Berna, M.R. Moreno, J. Villalain, Structure of the C-terminal domain of the pro-apoptotic protein Hrk and its interaction with model membranes, Biochim. Biophys. Acta 1768 (2007) 1659–1670.
[33] M. Giudici, R. Pascual, L. de la Canal, K. Pfüller, U. Pfüller, J. Villalaín, Interaction of viscotoxins A3 and B with membrane model systems: implications to their mechanism of action, Biophys J. 85 (2003) 971–981.
[34] H.G. Franquelim, S. Chiantia, A.S. Veiga, N.C. Santos, P. Schwille, M.A. Castanho, Anti-HIV-1 antibodies 2F5 and 4E10 interact differently with lipids to bind their epitopes, AIDS 25 (2011) 419–428.
[35] H.G. Franquelim, A.S. Veiga, G. Weissmuller, N.C. Santos, M.A. Castanho, Unravelling the molecular basis of the selectivity of the HIV-1 fusion inhibitor sifuvirtide towards phosphatidylcholine-rich rigid membranes, Biochim. Biophys. Acta 1798 (2010) 1234–1243.
[36] M. Lundin, H. Lindstrom, C. Gronwall, M.A. Persson, Dual topology of the processed hepatitis C virus protein NS4B is influenced by the NS5A protein, J. Gen. Virol. 87 (2006) 3263–3272.
[37] C. Welsch, M. Albrecht, J. Maydt, E. Herrmann, M.W. Welker, C. Sarrazin, A. Scheidig, T. Lengauer, S. Zeuzem, Structural and functional comparison of the non-structural protein 4B in Flaviviridae, J. Mol. Graph. Model. 26 (2007) 546–557.
[38] J. Guillen, A.J. Perez-Berna, M.R. Moreno, J. Villalain, A second SARS-CoV S2 glycoprotein internal membrane-active peptide. Biophysical characterization and membrane interaction, Biochemistry 47 (2008) 8214–8224.
[39] S. Shnaper, K. Sackett, S.A. Gallo, R. Blumenthal, Y. Shai, The C- and the N-terminal regions of glycoprotein 41 ectodomain fuse membranes enriched and not enriched with cholesterol, respectively, J. Biol. Chem. 279 (2004) 18526–18534.
[40] K. Salzwedel, J.T. West, E. Hunter, A conserved tryptophan-rich motif in the membrane-proximal region of the human immunodeficiency virus type 1 gp41 ectodomain is important for Env-mediated fusion and virus infectivity, J. Virol. 73 (1999) 2469–2480.
[41] A.J. Perez-Berna, A. Bernabeu, M.R. Moreno, J. Guillen, J. Villalain, The pre-transmembrane region of the HCV E1 envelope glycoprotein: interaction with model membranes, Biochim. Biophys. Acta 1778 (2008) 2069–2080.

[42] M. Lorizate, N. Huarte, A. Saez-Cirion, J.L. Nieva, Interfacial pre-transmembrane domains in viral proteins promoting membrane fusion and fission, Biochim. Biophys. Acta 1778 (2008) 1624–1639.
[43] M. Lorizate, I. de la Arada, N. Huarte, S. Sanchez-Martinez, B.G. de la Torre, D. Andreu, J.L. Arrondo, J.L. Nieva, Structural analysis and assembly of the HIV-1 Gp41 amino-terminal fusion peptide and the pretransmembrane amphipathic-at-interface sequence, Biochemistry 45 (2006) 14337–14346.
[44] R. Pascual, M. Contreras, A. Fedorov, M. Prieto, J. Villalain, Interaction of a peptide derived from the N-heptad repeat region of gp41 Env ectodomain with model membranes. Modulation of phospholipid phase behavior, Biochemistry 44 (2005) 14275–14288.
[45] J. Guillen, R.F. Almeida, M. Prieto, J. Villalain, Structural and dynamic characterization of the interaction of the putative fusion peptide of the S2 SARS-CoV virus protein with lipid membranes, J. Phys. Chem. B 112 (2008) 6997–7007.
[46] A.G. Krainev, D.A. Ferrington, T.D. Williams, T.C. Squier, D.J. Bigelow, Adaptive changes in lipid composition of skeletal sarcoplasmic reticulum membranes associated with aging, Biochim. Biophys. Acta 1235 (1995) 406–418.
[47] T.C. Laurent, K.A. Granath, Fractionation of dextran and Ficoll by chromatography on Sephadex G-200, Biochim. Biophys. Acta 136 (1967) 191–198.
[48] D.B. Fisher, C.E. Cash-Clark, Sieve tube unloading and post-phloem transport of fluorescent tracers and proteins injected into sieve tubes via severed aphid stylets, Plant Physiol. 123 (2000) 125–138.
[49] L. Yang, T.A. Harroun, T.M. Weiss, L. Ding, H.W. Huang, Barrel-stave model or toroidal model? A case study on melittin pores, Biophys. J. 81 (2001) 1475–1485.
[50] L.M. Contreras, F.J. Aranda, F. Gavilanes, J.M. Gonzalez-Ros, J. Villalain, Structure and interaction with membrane model systems of a peptide derived from the major epitope region of HIV protein gp41: implications on viral fusion mechanism, Biochemistry 40 (2001) 3196–3207.
[51] J. Villalain, Membranotropic effects of arbidol, a broad anti-viral molecule, on phospholipid model membranes, J. Phys. Chem. B 114 (2010) 8544–8554.
[52] R.M. Epand, Lipid polymorphism and protein–lipid interactions, Biochim. Biophys. Acta 1376 (1998) 353–368.
[53] T. Hayakawa, Y. Hirano, A. Makino, S. Michaud, M. Lagarde, J.F. Pageaux, A. Doutheau, K. Ito, T. Fujisawa, H. Takahashi, T. Kobayashi, Differential membrane packing of stereoisomers of bis(monoacylglycero)phosphate, Biochemistry 45 (2006) 9198–9209.
[54] J.L. Arrondo, F.M. Goni, Structure and dynamics of membrane proteins as studied by infrared spectroscopy, Prog. Biophys. Mol. Biol. 72 (1999) 367–405.
[55] D.M. Byler, H. Susi, Examination of the secondary structure of proteins by deconvolved FTIR spectra, Biopolymers 25 (1986) 469–487.
[56] R.N. Lewis, R.N. McElhaney, W. Pohle, H.H. Mantsch, Components of the carbonyl stretching band in the infrared spectra of hydrated 1,2-diacylglycerolipid bilayers: a reevaluation, Biophys. J. 67 (1994) 2367–2375.
[57] A. Blume, W. Hubner, G. Messner, Fourier transform infrared spectroscopy of $^{13}C{=}O$-labeled phospholipids hydrogen bonding to carbonyl groups, Biochemistry 27 (1988) 8239–8249.
[58] R.M. Epand, B. Gabel, R.F. Epand, A. Sen, S.W. Hui, A. Muga, W.K. Surewicz, Formation of a new stable phase of phosphatidylglycerols, Biophys. J. 63 (1992) 327–332.
[59] P. Garidel, A. Blume, W. Hubner, A Fourier transform infrared spectroscopic study of the interaction of alkaline earth cations with the negatively charged phospholipid 1,2-dimyristoyl-sn-glycero-3-phosphoglycerol, Biochim. Biophys. Acta 1466 (2000) 245–259.
[60] M. Dimitrova, I. Imbert, M.P. Kieny, C. Schuster, Protein-protein interactions between hepatitis C virus nonstructural proteins, J. Virol. 77 (2003) 5401–5414.
[61] R. Pascual, M.R. Moreno, J. Villalain, A peptide pertaining to the loop segment of human immunodeficiency virus gp41 binds and interacts with model biomembranes: implications for the fusion mechanism, J. Virol. 79 (2005) 5142–5152.
[62] F. Penin, V. Brass, N. Appel, S. Ramboarina, R. Montserret, D. Ficheux, H.E. Blum, R. Bartenschlager, D. Moradpour, Structure and function of the membrane anchor domain of hepatitis C virus nonstructural protein 5A, J. Biol. Chem. 279 (2004) 40835–40843.
[63] B. Bishe, G. Syed, A. Siddiqui, Phosphoinositides in the hepatitis C virus life cycle, Viruses 4 (2012) 2340–2358.
[64] M.S. Bretscher, S. Munro, Cholesterol and the Golgi apparatus, Science 261 (1993) 1280–1281.
[65] J. Gouttenoire, F. Penin, D. Moradpour, Hepatitis C virus nonstructural protein 4B: a journey into unexplored territory, Rev. Med. Virol. 20 (2010) 117–129.
[66] D.M. Jones, A.H. Patel, P. Targett-Adams, J. McLauchlan, The hepatitis C virus NS4B protein can trans-complement viral RNA replication and modulates production of infectious virus, J. Virol. 83 (2009) 2163–2177.
[67] H. Zhao, R. Sood, A. Jutila, S. Bose, G. Fimland, J. Nissen-Meyer, P.K. Kinnunen, Interaction of the antimicrobial peptide pheromone Plantaricin A with model membranes: implications for a novel mechanism of action, Biochim. Biophys. Acta 1758 (2006) 1461–1474.
[68] A.J. Perez-Berna, J. Guillen, M.R. Moreno, A. Bernabeu, G. Pabst, P. Laggner, J. Villalain, Identification of the membrane-active regions of hepatitis C virus p7 protein: biophysical characterization of the loop region, J. Biol. Chem. 283 (2008) 8089–8101.
[69] J. Koehler, N. Woetzel, R. Staritzbichler, C.R. Sanders, J. Meiler, A unified hydrophobicity scale for multispan membrane proteins, Proteins 76 (2009) 13–29.